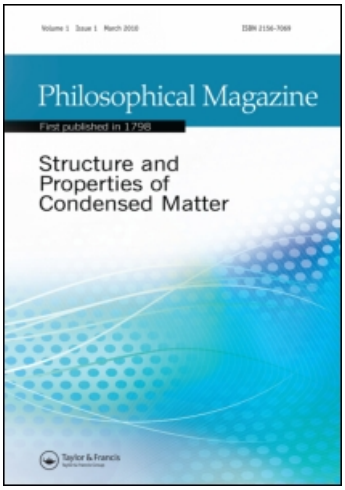

Philosophical Magazine
Publication details, including instructions for authors and subscription information:
http://www.informaworld.com/smpp/title~content=t713695589

Thermoelectric power factor of $RuSr_2GdCu_2O_8$

S. A. Saleh[ab]; E. M. M. Ibrahim[b]
[a] Physics Department, College of Science & Arts, Najran University, Saudi Arabia [b] Physics Department, Faculty of Science, Sohag University, Sohag 82524, Egypt

First published on: 06 December 2010

To cite this Article Saleh, S. A. and Ibrahim, E. M. M.(2011) 'Thermoelectric power factor of $RuSr_2GdCu_2O_8$', Philosophical Magazine, 91: 5, 841 — 849, First published on: 06 December 2010 (iFirst)
To link to this Article: DOI: 10.1080/14786435.2010.529091
URL: http://dx.doi.org/10.1080/14786435.2010.529091

Philosophical Magazine
Vol. 91, No. 5, 11 February 2011, 841–849

Taylor & Francis
Taylor & Francis Group

Thermoelectric power factor of $RuSr_2GdCu_2O_8$

S.A. Saleh[ab]* and E.M.M. Ibrahim[b]

[a]*Physics Department, College of Science & Arts, Najran University, P.O. 1988 Najran, Saudi Arabia;* [b]*Physics Department, Faculty of Science, Sohag University, Sohag 82524, Egypt*

(*Received 19 February 2010; final version received 27 September 2010*)

The influence of thermal treatment between 1273 and 1333 K in an oxygen atmosphere on the perovskite system $RuSr_2GdCu_2O_8$ was studied by X-ray diffraction (XRD), scanning electron microscopy, electrical resistivity and Seebeck coefficient measurements. The XRD patterns revealed that the phase purity depends on the sintering process. The samples were found to exhibit very small crystallite sizes in the nanometer range. The electrical resistivity was found to be strongly correlated with the heat treatment. The temperature dependence of electrical resistivity for one sample revealed semiconducting behavior, whereas the others exhibit metallic behavior. All the investigated samples exhibit a positive thermoelectric power, indicating the predominance of positive charge carriers. It was found that the power factor reaches a maximum value of $0.4 \times 10^{-4}\,W\,m^{-1}\,K^{-2}$ at 300 K.

Keywords: thermoelectric power; $RuSr_2GdCu_2O_8$ perovskite; sintering; resistivity; Seebeck coefficient

1. Introduction

Thermoelectricity, i.e. energy conversion between heat and electricity via thermoelectric phenomena in solids, has long been a fundamental issue in condensed matter physics and is currently attracting renewed interest as a promising energy-conversion technology, which is important for the efficient use of energy and the prevention of global warming. A broad search has been under way to identify new materials with enhanced thermoelectric properties. Several classes of materials are currently under investigation, including high-T_c superconductor oxides. The latter exhibit a large thermoelectric power (TEP) ($S = +100\,\mu V/K$), a low resistivity close to that of metals ($\rho = 0.2$ mΩ cm) and a rather low thermal conductivity ($\kappa = 2\,W\,m^{-1}\,K^{-1}$ at 300 K) [1], resulting in a high thermoelectric figure of merit ($Z = S^2/\rho\kappa$, where S is the Seebeck coefficient, ρ the electrical resistivity, and κ the thermal conductivity). Therefore, enhancing the thermoelectric properties of materials requires decreasing the electrical resistivity, improving the Seebeck coefficient or decreasing the thermal conductivity. To realize this, efforts have been directed towards microstructural and alloy design control of existing materials or finding new compounds. The sintering process strongly affects the electrical conductivity and Seebeck coefficient of oxides

*Corresponding author. Email: saleh2010_ahmed@yahoo.com

ISSN 1478–6435 print/ISSN 1478–6443 online

DOI: 10.1080/14786435.2010.529091
http://www.informaworld.com

and can be utilized to improve their thermoelectric properties [2]. Thermoelectric materials are used in power generation, for specialized applications in thermoelectric generators and also in refrigerators. Since the lattice thermal conductivity dominates over the electronic contribution for most materials used for room temperature applications, the single 'electronic' parameter that describes the efficiency of thermoelectric devices is the TEP, which is defined as S^2/ρ, where S is the Seebeck coefficient and ρ the electrical resistivity.

In this context, ruthenium-base oxides are promising candidates for use as thermoelectric materials. Although there have been an enormous number of studies [3–26] on the different physical properties of perovskite-type ruthenium oxides such as $RuSr_2GdCu_2O_8$ (Ru1212), a focus on their applicability as a thermoelectric material is very scarce.

The current study is an attempt, which shows to what extent we could successfully prepare pure samples of Ru1212 with a classical solid-state technique. Thereafter, a study of the effects of sintering process on the structural, electrical and thermoelectric properties of Ru1212 was made to evaluate these compounds as thermoelectric materials.

2. Experimental

The compound $RuSr_2GdCu_2O_8$ (Ru1212) was prepared by the solid state ceramic technique. Appropriate quantities of RuO_2, Gd_2O_3, CuO and $SrCO_3$, all of high purity, were thoroughly mixed, ground, and then calcined in air at 1233 K for 24 h, with one intermediate grinding. The starting materials were preheated at 873–1073 K. Then, the powders were pressed into pellets at a pressure of 5 ton cm^{-2} and subsequently sintered in nitrogen at 1303 K for 24 h. The sintering of these pellets was performed in oxygen at 1273 K for 72 h (sample A), at 1333 K for 72 h (sample B), and finally at 1333 K (sample C) for 100 h. The specimens were slowly cooled to room temperature.

Room temperature X-ray diffraction (XRD) spectra were obtained using a Brucker Axs-D8 Advance diffractometer with Cu K_α radiation in the 2θ range of 20–80° with the step of 0.04° and time per step 10 s. Scanning electron microscopy (SEM) combined with an energy dispersive X-ray analysis (EDXA) investigation was carried out with a JEOL JSM5300 instrument. Resistivity measurements were performed on bar-shape pieces cut out from the pellets with contact made with silver paint using a dc four-probe technique in the temperature range 80–300 K. The thermoelectric power factors of the samples were measured using a differential technique [27]. It should be noted that the same piece of sample was used for both measurements.

3. Results and discussion

The microstructural features of Ru1212 shown by the SEM images (Figure 1) are microcrystalline grains with variable sizes and shapes. Although varying in shape, they indeed consist of the same chemical compositions, as was confirmed from EDAX measurements. SEM analyses show grain homogeneity with clean grain

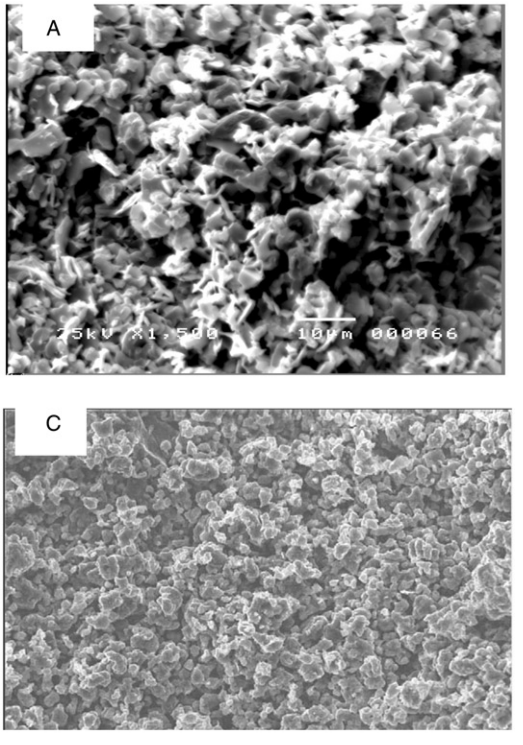

Figure 1. SEM photographs of samples A and C with the same scale.

boundaries. Very fine grain sizes are observed for sample C, whereas for sample A larger grains are detected with an average size of the order of 3μm, and some plate-like grains grown randomly. This random growth makes the pore volume increase and the apparent density of the sample decrease to $4.3\,g\,cm^{-3}$. The thermal treatment seems to play a role in making denser samples with a bulk density of $4.47\,g\,cm^{-3}$, as reported previously [3]. This enhancement of density may be due to decreasing of the macroscopic cracking. Therefore, heat treatment is an important process for maximizing the density.

X-ray diffractograms of the samples were analyzed to obtain information about various crystallographic features. A weak peak corresponding to $SrRuO_3$ (marked by a * in Figure 1) indicated the existence of impurity traces in sample A. However, with additional steps of sintering, the $SrRuO_3$ phase is diminished dramatically leading to high phase purity of Ru1212 for the sample C, which was sintered at 1333 K for 100 h, as can be seen in Figure 2c. This may be attributed to the fact that these conditions of sintering make the impurity layer thickness insufficient ($\leq$100 Å) to form diffraction peaks [27].

The peaks belonging to Ru1212 phase were indexed, showing that $RuSr_2GdCu_2O_8$ crystallizes in a tetragonal crystal structure. The values of the lattice constants, $a = 3.842$ Å and $c = 11.577$ Å, are comparable with those reported previously [23]. The intensity and peak positions of (103), (200), (213) and (206)

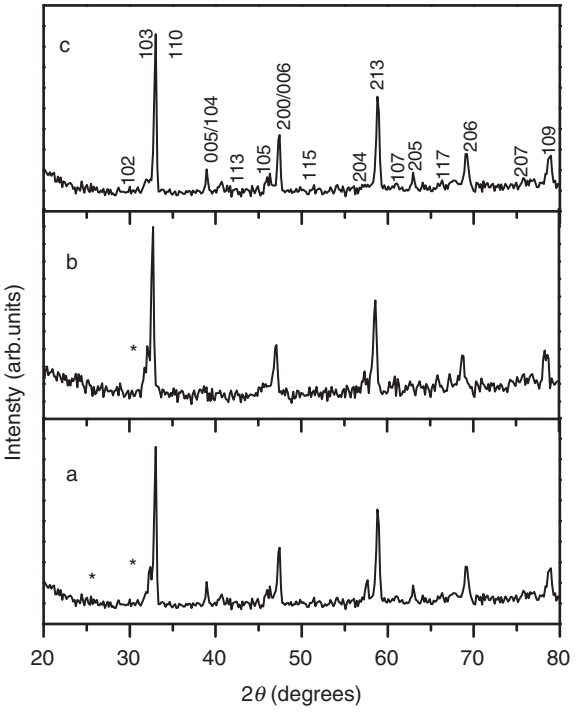

Figure 2. X-ray diffraction patterns obtained for tested samples.

reflections are in good agreement with the values reported in the literature [4,25,26]. The studied samples consist of a few slightly disoriented monocrystalline grains. The average grain sizes (G_s) of all samples were within the range 50.4–125.3 nm, as calculated from the main peaks (103) by using the well-known Scherrer formula [28],

$$G_s = \frac{k\lambda}{\beta \cos\theta}, \tag{1}$$

where the constant k depends upon the shape of the grain size ($=0.89$ assuming a circular grain), $\beta =$ full width at half maximum (FWHM) of the intensity versus 2θ profile, λ is wavelength of the Cu K_α radiation and θ is the Bragg diffraction angle. It was found that the grain size decreases due to the sintering process, which in turn suppresses cracking. This means that the sintering process seems to play an important role in increasing the grain orientation and grain connectivity. Obviously, the particle size that was observed by SEM is much larger than that determined from XRD since the former represents the size of aggregated nanocrystals of Ru1212.

Figure 3 shows the temperature dependence of the electrical resistivity (ρ) for $RuSr_2GdCu_2O_8$ in the range from 80 to 300 K. The resistivity decreases with increasing temperature over the measured temperature range, showing semiconducting-like behavior for sample A. However, sample B exhibits metallic behavior at higher temperature, whereas at low temperature the behavior changes to

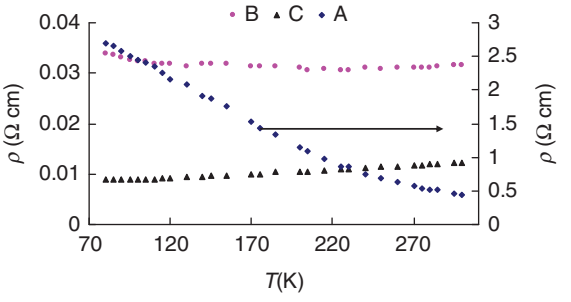

Figure 3. Electrical resistivity vs. temperature for investigated samples.

semiconducting. The ρ–T curve of sample C exhibits a metallic behavior over the whole temperature range of measurement. The electrical resistivity at 300 K was 0.448, 0.031, and 0.012 Ω cm for samples A, B, and C, respectively. Thus, one can conclude that the resistivity decreases when the sintering temperature increases, because of decreasing the macroscopic cracking and enhancement of the grain orientation and grain connectivity, in agreement the density, XRD, and SEM results. However, the electrical resistivity is not only determined by the degree of grain orientation but also depends on the carrier concentration (as discussed below).

An attempt was made to understand the semiconducting behavior in terms of conduction by electrons between localized states. Fitting of the resistivity curves could clarify the type of conduction and discriminate between pure thermally activated conductivity and variable range hopping (VRH) between localized electronic states.

For thermally activated conduction, the electrical resistivity can be written as a function of temperature, T, as follows $\rho = \rho_o \exp(E_\rho/k_B T)$, where E_ρ is the activation energy and ρ_o is a pre-exponential coefficient [29,30]. The calculated values of E_ρ from the linear portion of the ln (ρ)–$1/T$ curves were 4.5 and 3.5 meV for samples A and B, respectively. The difference in the activation energy values may be due to the sintering process.

The resistivity in Mott's three-dimensional variable range hopping [31] is given by

$$\rho = \rho_{om}(T/T_o)^{1/2} \exp(T_o/T)^{1/4}, \tag{2}$$

where $T_o = 21/(k_B N(E_F) a^3)$, in which a is the localization of length and $N(E_F)$ is the density of states. It is clear from Figure 3 that the thermal activation mechanism best matches the experimental data.

In the case of metallic state, $\rho(T)$ is well fit by the following empirical equation $\rho = \rho' + \alpha T$, where ρ' is the residual resistivity extrapolated to $T = 0$ (intercept) and the slope α represents the temperature coefficient of resistivity. The values of ρ' are 0.291 and 0.072 Ω for samples B and C, respectively. However, the values of α are 8×10^{-5} and 2×10^{-4} Ω cm K^{-1}. Thus, it can be concluded that the two parameters are strongly dependent on the sintering process. The decrease in residual resistivity and increase in temperature coefficient of resistivity with increasing sintering time can be ascribed to the enhancement of the Ru1212 phase, in agreement with XRD and SEM results.

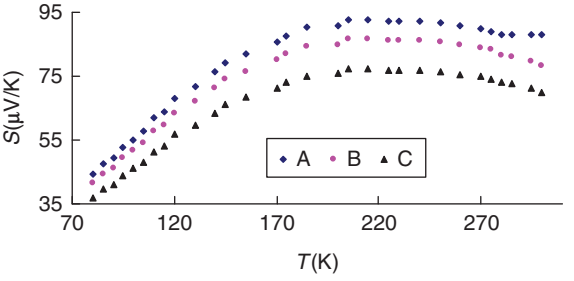

Figure 4. The temperature dependence of the Seebeck coefficient.

TEP measurements provide a useful tool to determine the electronic properties of samples because it is less sensitive to inter-grain impurities in comparison with the resistivity. In all the samples, the Seebeck coefficient was positive (see Figure 4) over the whole temperature range of measurement (80–300 K). The positive signs of S indicate that the materials investigated are p-type (the predominant carriers in these compounds are holes). All the samples exhibited similar temperature dependence: S increases with decreasing T, having a broad maximum at about 200 K and decreasing almost linearly with T below 150 K, similar to results for high-T_c cuprates.

In the temperature range 200–300 K, S increases linearly with a decrease in temperature with a negative slope. Thus, the Mott expression can be used to determine the Fermi energy [32,33]: $S = S_o - (\pi^2 {k_B}^2/3eE_F)T$, where S_o is a constant. Thus, a plot of S versus T should be a straight line; the Fermi level calculated from the slope was found to be 0.32 eV for sample A. The Fermi energy values were 0.2 and 0.197 eV [3] for samples B and C, respectively. This decrease of the Fermi energy with increasing sintering temperature reverses a significant dependency on the thermal treatment conditions. The temperature dependent of the Seebeck coefficient in sample A was analyzed using the Mott expression in which there is a local increase in the density of states (DOS) over a narrow energy range. The TEP data for samples B and C were analyzed from the standpoint of a two-band model with a linear T-term in which there is a narrow peak in the density of states of the charge carriers near the Fermi level. Hence, it can be concluded that the change in hole concentration has moved the Fermi energy.

The room temperature Seebeck coefficient was 88, 78, and 69.9 $\mu V\,K^{-2}$ for samples A, B, and C, respectively. The two variables S and ρ at room temperature are governed by the following formulae [34]:

$$S = \pm\frac{k_B}{e}\left[r + \frac{5}{2} + \ln\frac{2(2\pi m^* k_B T)^{3/2}}{ph^3}\right], \tag{3}$$

$$S = \pm\frac{K_B}{e}[r + \ln\rho] + C, \tag{4}$$

in which k_B is Boltzmann's constant, e the electronic charge, r the scattering parameter, m^* the effective mass, p the hole concentration, h is Planck's constant and

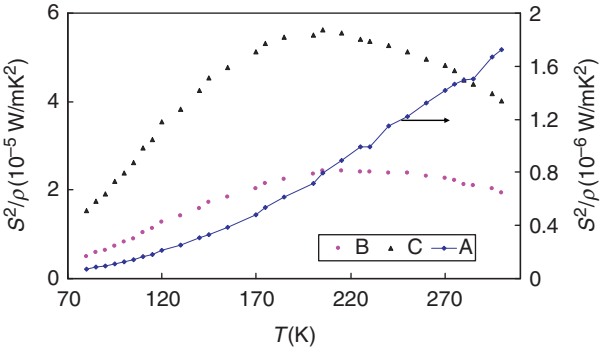

Figure 5. The temperature dependence of the power factor.

C is a constant. Also, it shows that the Seebeck coefficient is directly related to electrical resistivity when the scattering parameter is the same. As we know, S and ρ can be expressed as $\rho = 1/ne\mu$ and $S = \gamma - \ln n$ [35], where n is the carrier concentration, μ is the carrier mobility and γ is the scattering factor. As mentioned above, the density of the investigated samples increases with increasing sintering temperature. So, the carrier mobility, μ, increases or carrier effective mass decreases, and therefore the electrical resistivity and Seebeck coefficient decrease with increase in sintering temperature.

For the thermoelectric applications, both p- and n-type materials having high thermoelectric figures of merit are required simultaneously [36]. The power factor can be optimized as a function of the carrier concentration. The good performance of a thermoelectric material demands a high dimensionless figure of merit value, i.e. large power factor (PF) values and low thermal conductivity. The temperature dependence of the power factor of the samples calculated from the data of $S(T)$ and $\rho(T)$, is plotted in Figure 5. The PF of sample A increases with increasing temperature in the measured temperature range and the value reaches $1.7 \times 10^{-6}\,\mathrm{W\,m^{-1}\,K^{-2}}$ at 300 K. The power factor behavior corresponding to the both samples B and C has similar shape to that of the Seebeck coefficient one. It is worth noting that the sintering conditions are an efficient way to increase the room temperature power factor in these materials. The highest value at 300 K was $0.4 \times 10^{-4}\,\mathrm{W\,m^{-1}\,K^{-2}}$ and was recorded for sample C. The increase of power factor for Ru1212 samples resulted mainly from the decrease of the electrical resistivity, since the Seebeck coefficient was almost the same. On the other hand, these results confirm that preparing very fine-grained $RuSr_2GdCu_2O_8$ samples is very effective in improving the power factor of the thermoelectric material. The thermoelectric properties and mechanical characterization of the samples [3] are critical for material design and device fabrication [37].

4. Conclusion

$RuSr_2GdCu_2O_8$ (Ru1212) pellets with a tetragonal perovskite-type structure have been prepared using the solid state method followed by a high temperature sintering

in O_2 atmosphere. The XRD data indicate that the sintering process in flowing oxygen gas for a long time produced a reasonably pure Ru1212 phase. The electrical resistivity, TEP, and the thermoelectric power factor were measured as functions of temperature from 80 to 300 K. The electrical resistivity of samples shows either semiconductor or metallic behavior depending on the sintering conditions. The Seebeck coefficient measurements confirm that the carries are holes and the samples are underdoped cuprates. Due to the large TEP and the low resistivity close to that of metal, these materials are potential candidates for TE materials. The good thermoelectric performance increases well the efficiency of the TE generators and modules fabricated from the very fine powder, which is of great value in the TE industry.

References

[1] B. Raveau, J. Eur. Ceram. Soc. 25 (2005) p.1965.
[2] E. Meada and M. Ohtaki, Trans. Mater. Res. Soc. Jpn. 25 (2000) p.237.
[3] S.A. Saleh, S.M. Khalil and E.M.M. Ibrahim, Supercond. Sci. Tech. 20 (2007) p.372.
[4] I. Felner, U. Asaf, S. Reich and Y. Tsabba, Phys. C Supercond. 311 (1999) p.163.
[5] R.W. Henn, H. Friedrich, V.P.S. Awana and E. Gmelin, Phys. C Supercond. 341–348 (2000) p.457.
[6] I. Matsubara, N. Kida and R. Funahashi, J. Phys. Condens. Matter 13 (2001) p.5645.
[7] M. Li, M. Yu, Z. Wang, H. Yang, Y. Hu, Z. Chen, Z. Li and L. Cao, Phys. C Supercond. 382 (2002) p.233.
[8] A. Fainstein, E. Winkler, A. Butera and J. Tallon, Phys. Rev. B 60 (1999) p.R12596.
[9] J.L. Tallon, C. Bernhard, M.E. Bowden, P.W. Gilberd, T.M. Stoto and D.J. Pringle, IEEE Trans. Appl. Supercond. 9 (1999) p.1696.
[10] D.Z. Wang, H.I. Ha, J.I. Oh, J. Moser, J.G. Wen, M.J. Naughton and Z.F. Ren, Phys. C Supercond. 384 (2003) p.137.
[11] J.E. McCrone, J.L. Tallon, J.R. Cooper, A.C. MacLaughlin, J.P. Attfield and C. Bernhard, Phys. Rev. B 68 (2003) p.064514.
[12] G.K. Strukova, I.I. Zver'kova, L.A. Dorosinkii, D.V. Shovkun, V.N. Zverev and U. Topal, Phys. C Supercond. 387 (2003) p.359.
[13] M.R. Cimberle, R. Masini, E. Gilioli, F. Cordero, C. Artini, M. Ferretti, P. Mele and A. Martinelli, J. Magn. Magn. Mater. 272–276 (2004) p.1047.
[14] C. Bernhard, J.L. Tallon, E. Brücher and R.K. Kremer, Phys. Rev. B 65 (2000) p.R14960.
[15] C. Artini, M.M. Carnascilali, G.A. Costa, M. Ferretti, M.R. Cimberle, M. Putti and R. Masini, Phys. C Supercond. 377 (2002) p.431.
[16] M. Matvejeff, V.P.S. Awana, L.-Y. Jang, R.S. Liu, H. Yamauchi and M. Karppinen, Phys. C Supercond. 392–396 (2003) p.87.
[17] V.P.S. Awana, S. Ichihara, M. Karppinen and H. Yamauchi, Phys. C Supercond. 378–381 (2001) p.249.
[18] P. Mele, C. Artini, R. Masini, G.A. Costa, A. Hu, N. Chikumoto and M. Murakami, Phys. C Supercond. 412–414 (2004) p.196.
[19] L.T. Yang, J.K. Liang, Q.L. Liu, G.B. Song, F.S. Liu, J. Luo and G.H. Rao, Phys. C Supercond. 403 (2004) p.177.
[20] B. Lorenz, R.L. Meng, J. Cmaidalka, Y.S. Wang, J. Lenzi, Y.Y. Xue and C.W. Chu, Phys. C Supercond. 363 (2001) p.251.
[21] M. Očko, I. Živkovic, M. Prester, D. Drobac, D. Ariosa, H. Berger and D. Pavuna, J. Magn. Magn. Mater. 269 (2004) p.231.

[22] Z.H. Han, J.I. Budnick, W.A. Hines, P.W. Klamut, M. Maxwell and B. Dobrowski, J. Magn. Magn. Mater. 299 (2006) p.338.
[23] D.P. Hai, S. Kamisawa, I. Kakeya, M. Furuyama, T. Mochiku and K. Kadowaki, Phys. C Supercond. 357 (2001) p.406.
[24] R.L. Meng, B. Lorenz, Y.S. Wang, J. Cmaidalka, Y.Y. Xue and C.W. Chu, Phys. C Supercond. 353 (2001) p.195.
[25] L. Bauernfiend, W. Widder and H.F. Braun, Phys. C Supercond. 254 (1995) p.141.
[26] K. Otzschi, T. Mizukami, T. Hinouchi, J. Shimoyama and K. Kishio, J. Low Temp. Phys. 117 (1999) p.855.
[27] S.A. Saleh, Phys. C Supercond. 440 (2006) p.40.
[28] M.M. Ibrahim, E.M.M. Ibrahim, S.A. Saleh and A.M. Abdel Hakeem, J. Alloy Comp. 429 (2007) p.19.
[29] L. Martin-Carron, A. de Andres, M.J. Martinez-Lope, M.T. Casais and J.A. Alonso, Phys. Rev. B 66 (2002) p.174303.
[30] N.G. Bebenin, R.I. Zainullina, V.V. Mashkautsan, V.V. Ustinov and Y.M. Mukovskii Phys. Rev. B 69 (2004) p.104434.
[31] H.K. Barik, S.K. Ghorai, S. Bhattacharya, D. Kilian and B.K. Chaudhuri, J. Mater. Res. 15 (2000) p.1076.
[32] R.D. Barnard, *Thermoelectricity in Metals and Alloys*, Taylor & Francis Ltd, London, 1972.
[33] M.A. Rehman and A. Maqsood, Phys. C Supercond. 418 (2005) p.121.
[34] D.-B. Hyun, J.-S. Hwang, J.-D. Shim and T.S. Oh, J. Mater. Sci. 36 (2001) p.1285.
[35] X.A. Fan, J.Y. Yang, W. Zhu, H.S. Yun, R.G. Chen, S.Q. Bao and X.K. Duan, J. Alloy Comp. 420 (2006) p.256.
[36] M. Rowe, *CRC Handbook of Thermoelectrics*, CRC Press, New York, 1995, p.19.
[37] F. Ren, E.D. Case, E.J. Timm, E. Lara-Curzio and R.M. Trejo, Acta Mater. 58 (2010) p.31.